**CoreTek, Inc.**

*Advanced Photonic Devices and Systems*

738 Main Street, No. 247
Waltham, MA 02154

Voice: (617) 926 3608
FAX: (617) 926 9674
e-mail: 5959040@mcimail.com

September 19, 1994

# Final Report

## "Commercial Photorefractive Devices Using Nonstoichiometric III-V Semiconductors"

**Submitted To:**



AFOSR/PKA
110 Duncan Ave, Suite B115
Bolling AFB DC

**AFOSR Contract No:** F4962-94-C-0037, DEF
**Contract Effective Date:** June 15, 1994
**Reporting Period:** July 15 to Dec.15
**CoreTek, Inc. Job No.:** AFOSR9401

**Program Manager:**

Dr. Gerald L. Witt

**Prepared by:**

Parviz Tayebati, Ph. D.
CoreTek, Inc.

# REPORT DOCUMENTATION PAGE

Form Approved
OMB No. 0704-0188



| 1. AGENCY USE ONLY (Leave blank) | 2. REPORT DATE | 3. REPORT TYPE AND DATES COVERED |
|---|---|---|
| | | FINAL |

**4. TITLE AND SUBTITLE**
(SBIR) Commercial Photorefractive Device Using Nonstiochiometric III-V Semiconductors

**5. FUNDING NUMBERS**
XXXXXXX

**6. AUTHOR(S)**
Dr Tayebati

65502F
3005/SS

**7. PERFORMING ORGANIZATION NAME(S) AND ADDRESS(ES)**
CoreTek, Inc
Waltham, MA 02154

**8. PERFORMING ORGANIZATION REPORT NUMBER**
AFOSR-TR 95 0127

**9. SPONSORING MONITORING AGENCY NAME(S) AND ADDRESS(ES)**
AFOSR/NE
110 Duncan Avenue Suite B115
Bolling AFB DC 20332-0001



**10. SPONSORING MONITORING AGENCY REPORT NUMBER**
F49620-94-C-0037

**11. SUPPLEMENTARY NOTES**

**12a DISTRIBUTION AVAILABILITY STATEMENT**
APPROVED FOR PUBLIC RELEASE: DISTRIBUTION UNLIMITED

**12b. DISTRIBUTION CODE**

**13. ABSTRACT** (Maximum 200 words)

SEE FINAL REPORT ABSTRACT

**14. SUBJECT TERMS**

**15. NUMBER OF PAGES**

**16. PRICE CODE**

| 17. SECURITY CLASSIFICATION OF REPORT | 18. SECURITY CLASSIFICATION OF THIS PAGE | 19. SECURITY CLASSIFICATION OF ABSTRACT | 20. LIMITATION OF ABSTRACT |
|---|---|---|---|
| UNCLASSIFIED | UNCLASSIFIED | UNCLASSIFIED | UNCLASSIFIED |

*Phase I Proposal Abstract:*

Non-stoichiometric (NS) III-V materials offer a unique opportunity to technologies such as optoelectronic based photorefractive devices that require both short carrier diffusion length and enhanced electrooptic properties. With the ability to process 2D data at rates two orders of magnitude higher than the capability of digital electronics, these devices will facilitate commercialization of enormously marketable technologies such as ultra high speed object recognition, defect and parts recognition in assembly lines and supermarkets, etc.

CoreTek, Inc. proposes a novel commercial photorefractive device that takes advantage of the unique properties of NS-GaAlAs. With diffraction efficiency > 8%, a response time of 1μs and a spatial definition of 3μm, these devices are ideal for the practical applications noted. In Phase I, our team of experts, Dr.s P. Tayebati of CoreTek, D. D. Nolte of Purdue University and W. D. Goodhue of U. Mass. Lowell, will test the feasibility of the approach by fabricating and testing sample devices. In Phase II, CoreTek will optimize these devices for specific applications and make them commercially available as off-the-shelf products.

# FINAL REPORT

## "Commercial Photorefractive Devices Using Nonstoichiometric III-V Semiconductors"

### *1. EXECUTIVE SUMMARY*

In this Phase I program CoreTek, Inc. has developed the first all-semiconductor photorefractive spatial light modulator (PR-SLM) using Low-Temperature-Grown (LTG) GaAlAs materials. Taking advantage of unique electronic and electrooptic properties of LTG-GaAlAs materials alone CoreTek's novel PR-SLM device (shown in Figure 1) presents technology breakthroughs in the following respects:

- *High Spatial Resolution*: A record spatial resolution of 5μm compared to 40μm respectively for today's state-of-the-art by AT&T and others (see Table 1). This means over 50 times higher processing throughput per unit area.

- *Fast Response Time*: A record fast response time of 3μs compared to 30μs for today's state-of-the-art by AT&T (@ 0.1W/cm$^2$). This means a factor of twenty improvement in device speed.

- *Longest Storage Time*: Storage time of over 10ms, compared to 20μs storage time in AT&T's devices.

- *Monolithic Structure:* Going well beyond the goals of Phase I, we exploited the extraordinary semiinsulating properties of LTG-GaAlAs to fabricate the first all LTG-GaAlAs PR-SLM device in a *semi-monolithic* form. This is a significant technology breakthrough allowing fabrication of *fully monolithic* devices in Phase II.

This technological breakthrough achievement coupled with the inherent low production cost offer an enabling technology for commercial optical image processing applications such as *optical pattern recognition*. Optical image correlation is a critical technology in almost any situation where recognition of objects and patterns is required. A short list of such applications include:

1. Automatic assembly lines, e.g. chip assembly and circuit board manufacturing
2. Quality control & defect recognition
3. Finger print and figure identification
4. Military target recognition, etc

In a Phase II we will use our PR-SLM device, in combination with the top-of-the-line electrically addressed SLMs and smart detectors, to build a prototype compact optical correlator system (see Figure 2). Our photorefractive based image correlator presents the following advantages:

- Taking advantage of the *nonlinear* photorefractive properties of our PR-SLM, the proposed correlator is *seven* times less sensitive to noise than previously proposed optical correlators.

- Limited by the frame rate of top-of-the-line electrically addressed SLMs, and smart detector arrays, our system will be capable of processing 256x256 array size images in 0.1ms. This is more than two orders of magnitude faster than commercially available state-of-the-art COGNEX 3400 series machine vision technology capable of correlating images in 58ms.

**Table 1. Comparison of CoreTek's LTG-GaAlAs Photorefractive SLM Device with Competing Technologies**

| | *Frame Speed* | *Diffraction Efficiency* | *Dynamic Range* | *Spatial Resolution* | *Manufacturability & Cost Issues* |
|---|---|---|---|---|---|
| ***Ferroelectric Liquid Crystal SLM (Optically Addressed)*** | 30μs | 20% | 50:1 | 20μm-40μm | Low yield devices<br>Nonreproducible characteristics<br>High Cost~ $15,000/device |
| ***Ferroelectric Liquid Crystal SLM] (Electrically Addressed)*** | 1ms | 70% | 50:1 | 30μm | Sensitive to low levels of dopants<br><br>High Cost~$3000/sample |
| ***Magnetooptic Spatial Light Modulator*** | 1 ms | 10% | 100:1 | 60μm | High currents (130mA) required for switching limits practical applications<br><br>Cost >$10,000 |
| ***GaAs (Bulk)*** | 10 ms[(a)] | 5% | 100:1 | 0.2μm | Sensitive to low levels of dopants |
| ***AT&T's MQW Based Phtorefractive Device*** | 10 μs[(a)] | 1.5% (output efficiency) | >1000:1 [(b)] | 20μm -30μm | Hybrid device<br>Requires combination of MBE and multiple RFD sputtering<br>Current fabrication cost >$1000/piece |
| ***CoreTek's LTG-GaAlAs Photorefractive Device*** | | | >1000:1 [(b)] | | Monolithic semiconductor device<br>Requires a single MBE growth<br>**Fabrication Cost:** |
| ***Phase I Result:*** | ~ 3 μs [(a)] | 3% (output efficiency) | | 3μm -6μm | **<$600/piece** |
| ***Phase II Target:*** | < 0.5 μs[(a)] | 4%-8% (input efficiency) | | 2μm -3μm | **<$100/piece** |

(a) @ 100mW/cm$^2$
(b) Determined by the background radiation

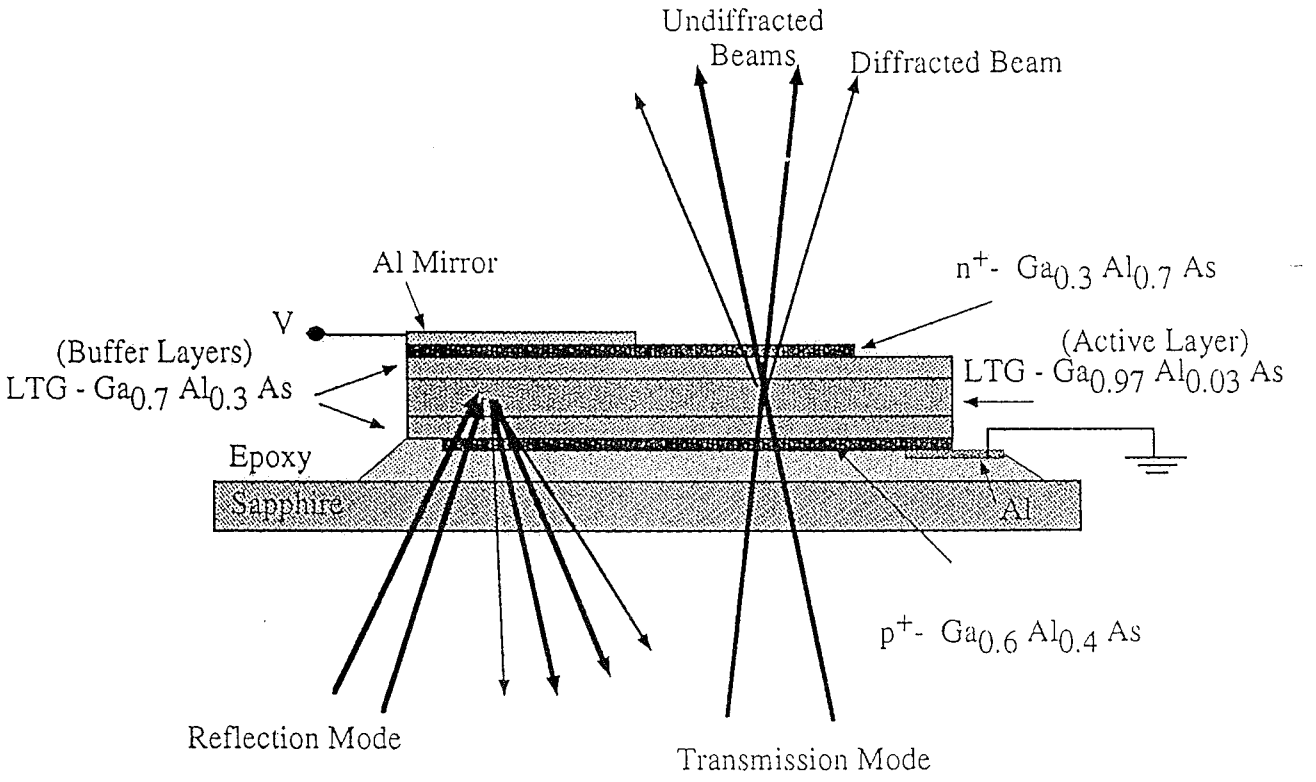


**Figure 1. CoreTek's "Semi-Monolithic" Device Structure.**

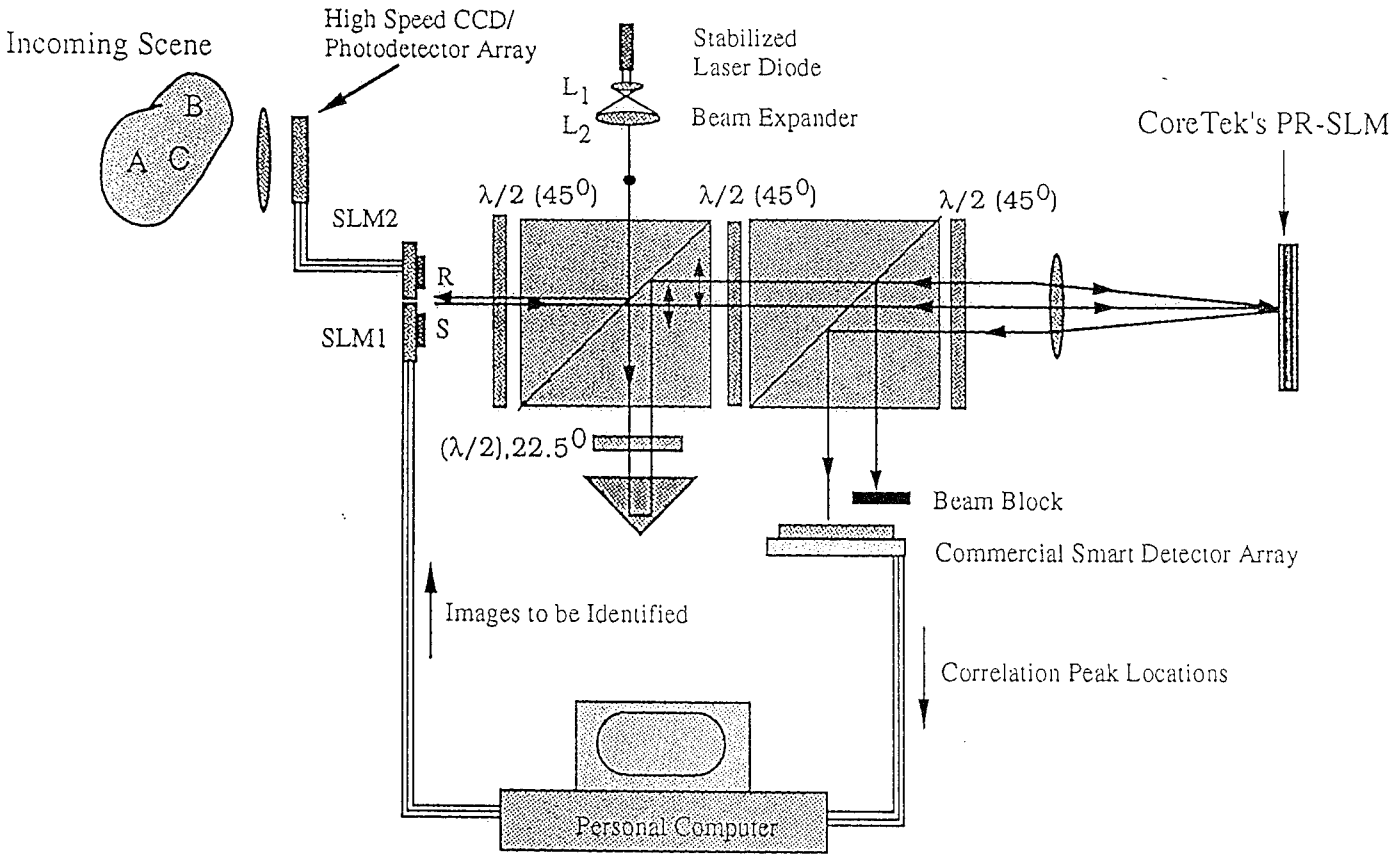


**Figure 2. A Novel Ramn Natho Optical Correlator.**

## 2. PHOTOREFRACTIVE SPATIAL LIGHT MODULATORS (PR-SLM)

### 2.1 Technical Background

In this section we will describe the structure and basic operation of PR-SLMs devices in general and our proposed device in particular. The aim is to describe the shortfalls of standard PR-SLM devices, the motivation for our proposed approach and our approch removed these shortfalls.

Figure 3 depicts the device first described by A. Glass et al. at AT&T laboratories [1]. Inhomogeneous spatial modulation of light creates a corresponding charge screening modulation and a large electroabsorption and electrorefraction modulation in the MQW layer. The large magnitude of the electroabsorption causes moderate diffraction efficiency $\eta$ defined as the first order Raman-Nath diffracted beam divided by the incoming beam intensity given by,

$$\eta = e^{-\alpha L} \times \left[ \sin^2\left( \frac{\pi \Delta n L}{\lambda \cos\left(\theta_{in}\right)} \right) + \sinh^2\left( \frac{\Delta \alpha L}{4\lambda} \right) \right] \qquad (1)$$

where $\lambda$ is the wavelength of operation, $\Delta\alpha$ is the electroabsorption, $\Delta n$ is the electrorefraction, L is the thickness of the device and $\theta_{in}$ is the angle of refraction. It can be shown that optimum diffraction efficiency for a pure absorption grating is approximately 3.7% for a case where the absorption modulation depth is maximum $\Delta\alpha=\alpha$.

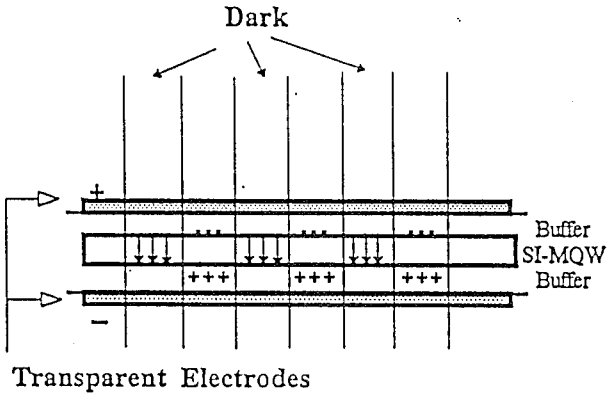


**Figure 3. The Schematic of a PR-SLM as first proposed by A. M. Glass of AT&T [1]**

In addition to electroabsorption in MQWs, there is a large electrorefraction $\Delta n$ that is approximately 0.01 for every $\Delta\alpha$=1000 $cm^{-1}$ [2,3]. This contribution being large, significantly enhanced the diffraction efficiency. The observed 1.5% diffraction efficiency in these devices is consistent with independent measurements of $\Delta n \sim 0.015$ and $\Delta\alpha \sim 1750$ $cm^{-1}$ below the band edge in conventional MQWs [4,5].

## 2.2. Poor spatial resolution in the perpendicular geometry MQW device

In contrast to the low quantum efficiency of the charge carrier transport normal to the direction of the MQWs, these carriers move quite freely in the parallel direction. The high degree of in-plane freedom decreases the spatial resolution of the system to the extent that in most reported cases the diffraction efficiency drops quite fast below 20-40μm [1,2,3]. The finest grating spacing is given by,

$$\Lambda = L_D = \sqrt{\frac{k_B T \mu \tau}{e}}, \qquad (4)$$

where $L_D$ is the bipolar diffusion length, $\mu\tau$ is the effective bipolar mobility-lifetime product. Measumement of approximately 20 to 40μm minimum fringe spacing is consistent with the in-plane carrier diffusion length. This value of spatial resolution is far less than the diffraction limited value of 1-2μm that is required for compact optical correlatros. In order to improve this property it is necessary to reduce the carrier diffusion length to less than 2μm. It is the main trust of this project to show that LTG-GaAlAs materials indeed can provide this property while not affecting other properties such as diffraction efficiency and the response time.

## 2.3. Model of Response Time

The response time of MQW photorefractive device is determined by how long it take to generate and transfer enough charges from one face of the device to the other to screen the field as shown in Figures 1. Assuming a quantum efficiency of Q, the response time of the device is approximately,

$$\tau = \frac{\varepsilon E h\nu}{2QeL\alpha I_0} \qquad (2)$$

where, is absorption coefficient, E is the electric field e is the dielectric constant, L is materials thickness, $I_0$ is intensity and hν is photon energy. Using characteristic numbers for MQWs: $\alpha=10^4$ cm$^{-1}$, E= 80kV/cm and L=1μm thick sample, we find $\tau \sim 40$ ns. This is approximately 25 times smaller than what is observed experimentally by Partovi [2-4] and is blamed on the low Q ~0.04 of quantum wells due to multiple trapping. As we shall describe below using LTG-GaAlAs materials as the writing layer allow for improved response time owing to slightly better quantum efficincy.

## 2.4. Fabrication Process

An important issue is the fabrication of MQW based devices. As discussed above in the final form such devices consists of an ion implanted MQW based device sandwiched between two layers of oxides ($Si_3N_4$/ITO) on either side and the entire structure is epitaxially lifted onto sapphire using an epoxy supported Vander-Walls bonding. This process is "hybrid" in nature and consumes much time and has low yield. In principle it is much prefered to develop a device structure that needs no oxide deposition and can be grown "monolithically". This has been accomplished for the first time in this Phase I program. The details are described below.

## 3. DESCRIPTION OF PHASE I GOALS

As desciribed in the last section poor spatial resolution and hybrid structure are two main shortfalls of MQW based photorefractive devices. In Phase I proposal CoreTek Inc. Proposed to develop a novel reflection-type thin film photorefractive device based on non-stoichiometric (NS) III-V as a key component for niche high speed 2D optical processing applications such as optical correlation. Our originally proposed device, shown in Figure 4, offers an order of magnitude advantage in spatial resolution and a factor of five advantage in diffraction efficiency over present multiple quantum well (MQW) based devices [1,2] while offering the same high speed of 1μs (at $1W/cm^2$). As proposed, the device structure did not address the "hybrid" versus "monolithic" structure. This was addressed during the Phase I program and is described in section 4.1

### 3.1. CoreTek's Innovative Thin Film LTG-GaAlAs Photorefractive Device Structure

CoreTek Inc's innovative reflection-type device, circumvents the poor spatial resolution problem by recording the photorefractive grating in a LTG- $Ga_{0.97}Al_{0.03}As$ thin film. (Figure 4). The high density of trapping sites in LTG- $Ga_{0.97}Al_{0.03}As$ layer (grown at 250 $^oC$) result in exceptionally high spatial resolution, on the order of ~ 0.5μm (compared to 40 μm for the AT &T devices). This phenomenon renders the device suitable for high definition applications.

In our proposed device higher diffraction efficiencies are expected because of (a) the enhanced near bandedge electroabsorption in GaAlAs , with absorption changes as high as 4000 $cm^{-1}$, and (b) use of a metallic deposited mirror at the exit side of the device to provide double pass capability the reading beam (and to the writing beam). Within the range of our parameters, increasing the interaction length increases the diffraction efficiency by up to a factor of four.

The structure of the device shown in Figure 4 consists of the following layers:

- Layer A: A LTG-$Ga_{0.97}Al_{0.03}As$ layer [8,9] with a zero-field energy band gap at 850 nm. This layer plays the double role of high speed recording layer and the electrooptic layer. LTG-GaAlAs is a recently developed material with high density of traps enabling 0.5μm spatial resolution (compare with 40μm in MQWs)

- Layer B: A dielectric buffer layer with high dielectric constant. In Phase I we will consider phosphate glass and silicon nitride Si3N4.

- Layer C: This layer is a high reflectivity sputtered silver mirror permitting the writing beam as well as the readout beams to double pass through the nonlinear/recording medium (LTG-GaAlAs). This will quadruple the diffraction efficiency and enhance the quantum efficiency of writing process by fifty percent.

- Layer D: $n^+$-GaAlAs, grown monolithically with the LTG-GaAlAs layer, is the top electrode. Alternatively, this layer can be sputtered indium tin oxide (ITO layer deposited after growth. On top of these layers an antireflection coating is deposited to increase the modulation index and the diffraction efficiency.

### 3.2. Basic Operation and Specifications of Our Proposed Photorefractive Device

The operation of the proposed device, depicted in Figure 4, is similar in many ways to MQW based devices described elsewhere [1,2,4,5] and is as follows:

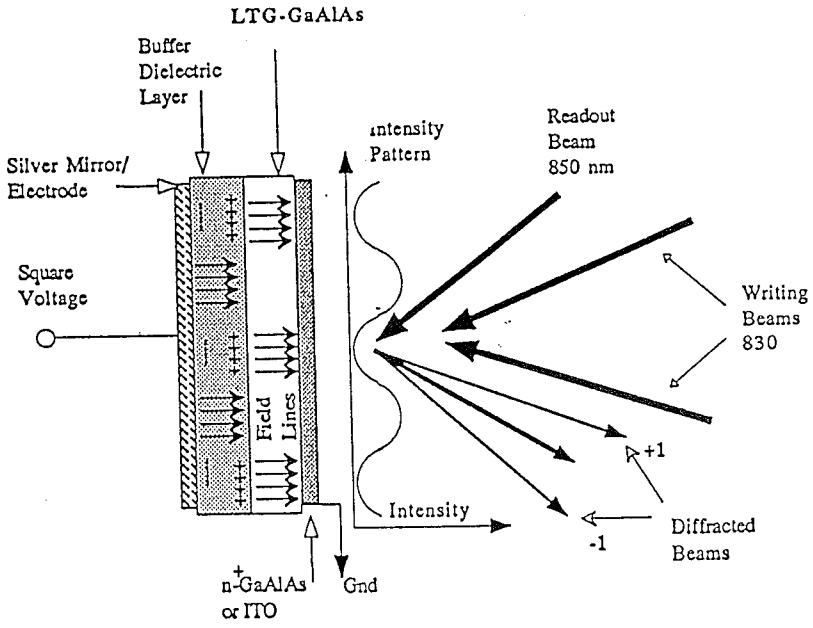


**Figure 4. (a) Schematic Of CoreTek's Semiconductor Photorefractive Device Originally Proposed for Phase I. (b) The basic operation of the device involves writing a conductivity grating, using 830nm-850 nm, in the LTG-GaAlAs layer which spatially modulates in this layer via screening. The readout beam is diffracted by enhanced double passing through the this layer.**

Two writing beams (830-850 nm) interfere in layer A (LTG-GaAlAs) and create a photoinduced charge grating. Application of a 10V step potential across the device at this time moves the photoinduced charges in such a way as to screen the electric field in the bright areas in this layer in approximately 1μs. The voltage in the bright regions of the LTG area is reduced to near zero, from approximately 5 V, and the and the field in the buffer layer area is increased from its t=0 value of 5 V, to a maximum of 10V.

As in the case of AT&T's MQW based devices, the spatial modulation of the electric field in the LTG-GaAlAs, causes a modulation electroabsorption ($\Delta\alpha$) and electrorefraction ($\Delta n$). The bandedge electrooptic modulation is the central mechanism for the four-wave mixing process in this device. The photorefractive grating is then read out using an 850 nm beam which enters the device and diffracts off the photorefractive grating in double passing through the device. The silver mirror provides over 97% reflection [9], adequate for our application. The intensity of the reflected beam must be low, compared to the writing beams, to not affect writing process. In case the readout and the writing beam have the same wavelength, the readout beam can be chosen to be of a different polarization wavelength so as to allow separating it from the writing beams. Using the reported electroabsorption data in LTG-GaAlAs [4,6] shown in Figure 5 and the above explanation, we calculate the spectral response of the diffraction efficiency $\eta$ of approximately 8% (see section e).

The silver mirror is an important dual role in this device:

(a) By reflecting the readout beams, this mirror allows double passing the readout beam through the nonlinear medium. Increasing the interaction length by a factor of 2, thus enhancing the diffraction efficiency by nearly a factor of 4.

(b) The mirror also reflects back the writing beams. Upon reflection, the remaining photons are again subject to absorption in the recording area, increasing the carrier generation rate and therefore the speed of the device by almost a factor of 1.5 .

*- Arsenic Quantum Dots: Key to Achieving High Spatial Resolution and Sensitivity*

The key to achieving high spatial resolution in our novel photorefractive device is in using Arsenic precipitate quantum dots produced in Low-Temperature Grown (LTG) GaAlAs thin films (Figures 1, 4). Arsenic Quantum Dots in the LTG layer confine the photocarriers generated by the interfering recording beams. By varying the growth and anneal temperatures the size and spacing of the As precipitants and therefore the spatial definition of the device can be tuned. In our approach the LTG-GaAlAs layer is used to record charge-holographic features as fine as 6 μm (theoretically down to 2μm is possible). Holographic readout process is then achieved via the large electrooptic effect in a directly coupled AlAs/GaAs multiple quantum well structure that is grown monolithically on top of the LTG recording layer. The coupling is achieved via charge screening caused The recorded charge-hologram spatially modulates the electrooptic effect (Quantum Confined Stark Effect) in the MQW layer allowing efficient holographic readout at the exciton wavelength.
In Table 2 innovative techniques used in our LTG-GaAlAs device and advantages they offer is summarized.

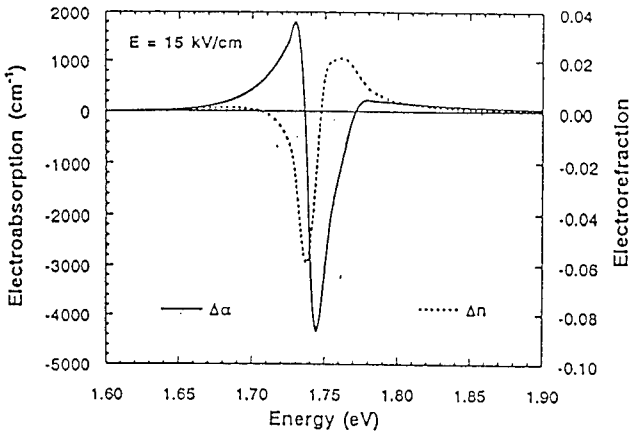


**Figure 5 . The electroabsorption spectrum of LTG-GaAlAs [4].**

**Table 2. CoreTek's Innovative Techniques Used In the LTG-GaAlAs device And Advantages They Offer.**

| CoreTek's Novel Technique | Advantage |
|---|---|
| • Using LTG-GaAlAs as Recording Medium | • Order-Of -Magnitude Improvement of the Spatial Resolution Compared to MQW devices |
| • Using LTG-GaAlAs as Recording Medium | • Enhanced Diffraction Efficiency |

| | |
|---|---|
| • Incorporation of silver Mirror | • Enhanced Diffraction Efficiency Double Passing Read Beam<br>• Increase Response time (50%)<br>• Enhance Writing Efficiency |

## 4. PHASE I RESULTS

### 4.1 Advanced "Semi-Monolithic" Design

The proposed device in Figure 4 shares similar fabrication problems as the original MQW based device. In these devices there is a need for deposition of two oxide layers followed by substrate removal and again oxide deposition. In addition electrode contacting is difficult and involves further etching process.

In Phase I *we took advantage of the semiinsulating properties of the LTG-GaAlAs materials to develop a photorefractive technology that can be easily extended to fabricate fully monolithic devices. The key element in this breakthrough was the use of wide band gap LTG-GaAlAs materials as the dielectric buffer layers.* The electrodes could then be grown epitaxially below and above the structure. The structure of the as grown device shown in Figure 1 is as follows.

| Layer | Composition | x | Thickness (μm) | Doping | Growth Temperature (degrees) | Role |
|---|---|---|---|---|---|---|
| 1 | $p^+$-$Ga_{1-x}Al_xAs$ | 0.6 | 0.25 | $1\times10^{19}$ | 600 | Top Electrode |
| 2 | i-$Ga_{1-x}Al_xAs$ | 0.3 | 1 | - | 310 | Buffer Layer |
| 3 | i-$Ga_{1-x}Al_xAs$ | 0.03 | 1.5 | - | 310 | Photorefractive Layer |
| 4 | i-$Ga_{1-x}Al_xAs$ | 0.3 | 1 | - | 310 | Buffer Layer |
| 5 | $n^+$-$Ga_{1-x}Al_xAs$ | 0.3 | 0.25 | $1\times10^{18}$ | 600 | Bottom Electrode |
| 6 | i-$Ga_{1-x}Al_xAs$ | 0.7 | 0.5 | - | 600 | Etch Stop |
| 7 | i-$Ga_{1-x}Al_xAs$ | 0 | 0.05 | - | 600 | Growth Buffer |
| 8 | i-$Ga_{1-x}Al_xAs$ | 0 | 300 | - | - | Substrate |

The top five layers constitute the photorefractive structure: The layer number 3 is the hart of the device where the photorefractive grating is recorded and readout. The 3% aluminum in this layer shifts the band gap to near 830nm where the device operates. Layers 2 and 4 are photorefractive buffer layers introduced for the first time and as an alternative to the usual

oxides used in previous work. Introduction of these epitaxial layers allows fabrication of such devices in a single run without having to resort to multiple deposition procedures. The layers 1 and 5 are p- and n-type wide band gap electrodes allowing application of an electric field. Before the development of this device Indium Tin Oxide had to be used in two post deposition tasks. Using LTG-GaAlAs as buffer layers allows epitaxial growth of the electrode layers. In this form the device is semi-monolithic since the substrate must still be removed. For this reason a high aluminum content layer is grown below before the structure (layer 6) to allow substrate removal.

### 4.2 Fabrication and Testing of Novel LTG-GaAlAs Photorefractive Devices in Transmission and Reflection Modes

Following growth, the sample is first diced into 5×5 mm samples and glued from the top $p^+$ layer to the sapphire substrate. Before gluing the sample, three sides of the top $n^+$-layer were recessed using standard photolithography and $NH_4OH:H_2O_2$ (1:45) etchant. We propose to use EpoTech.102 epoxy to bond the sample to the sapphire substrate. This epoxy is recognized for producing high quality results in this type of applications. Once the epoxy is set, the substrate is lapped down and chemically etched using $NH_4OH:H_2O_2$ (1:45) etchant. This selective etch stops at the etch stop. The etch stop will then be removed by HF:H2O (1:10) etchant. This etchant etches Ga1-xAlxAs materials with $x > 0.45$ at a rate 107 times faster than materials with $x<0.45$. This extremely high degree of selectivity leaves the $p^+$-GaAlAs layer in excellent high condition. We will then recess three edges of the $p^+$- layer by standard photolithography and chemical etching. This recessing of the $p^+$- and the $n^+$-layers are done to avoid possible shorting at the edges. The unrecessed $n^+$ and $p^+$ edges are in opposite sides and allow, by means of further etching and photolithogrophy and gold deposition, to electrically access the top and the bottom layers

Figure 1 shows the structure of the prototype device we fabricated and tested in Phase I. In the final form the device is a p-i-n diode structure that is bonded to a sapphire substrate. The film quality and device raggedness are excellent. After characterization of device performance in the transmission mode, an aluminum mirror was deposited on part of the device to study its behavior in the reflection mode. The latter is discussed later in this section. In summary these results clearly showed the feasibility of our innovative approach of using LTG-GaAlAs for building high resolution photorefractive devices.

In what follows we describe the results of our Phase I effort so far including a complete characterization in transmission and reflection. These experiments were done by CoreTek at the Physics Department of U. Mass Lowell in collaboration with Professor J. Kumar. Independent characterization of a sister sample was performed at Purdue University by Prof. David Nolte. The samples were grown by Professor Mike Melloch.

*4.2.3. Transient electroabsorption experiments* confirmed the combined effects of electroabsorption (in the electrooptic LTG-$Ga_{0.97}Al_{0.03}As$ layer) and charge screening (by the buffer LTG-$Ga_{0.7}Al_{0.3}As$ layers). In these experiments a single laser beam, with a wavelength close to the band edge of the $Ga_{0.97}Al_{0.03}As$ layer, is passed through the sample (Figure 1 shows the structure of the device in its final form). A step voltage is then applied. In a material with no charge screening effect one would expect a step-like change in transmission lasting as long as the voltage is on. In our photorefractive structure the charges created in the middle layer (LTG-$Ga_{0.97}Al_{0.03}As$ ) are swept to sides and trapped at the buffer layer (LTG-$Ga_{0.7}Al_{0.3}As$) interfaces. In time (microseconds), this process screens the field from the LTG-$Ga_{0.97}Al_{0.03}As$ region. As a result the transmission undergoes a fast initial change and eventually settles to its initial value as charges screen the field. We clearly

see this effect; in fact the effects were quite large, as much as 50% (corresponding to $\Delta\alpha \sim -2700 cm^{-1}$). Figures 6 shows oscilloscope pictures of the effect for wavelengths just above (positive effect) and just below the band edge (negative effect). Figure 7 shows the wavelength dependence of the effect. The positive and negative electroabsorption effects are consistent with the Franz-Keldysh oscillations.

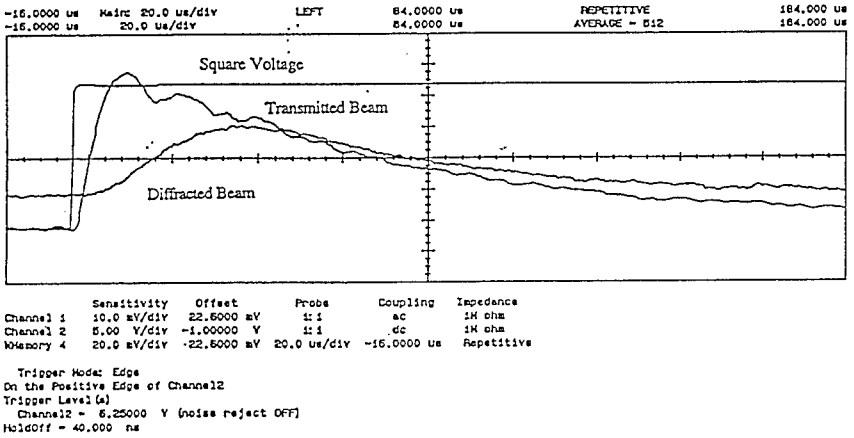


**Figure 6 Transient Electroabsorption Confirms a Healthy Device Structure**

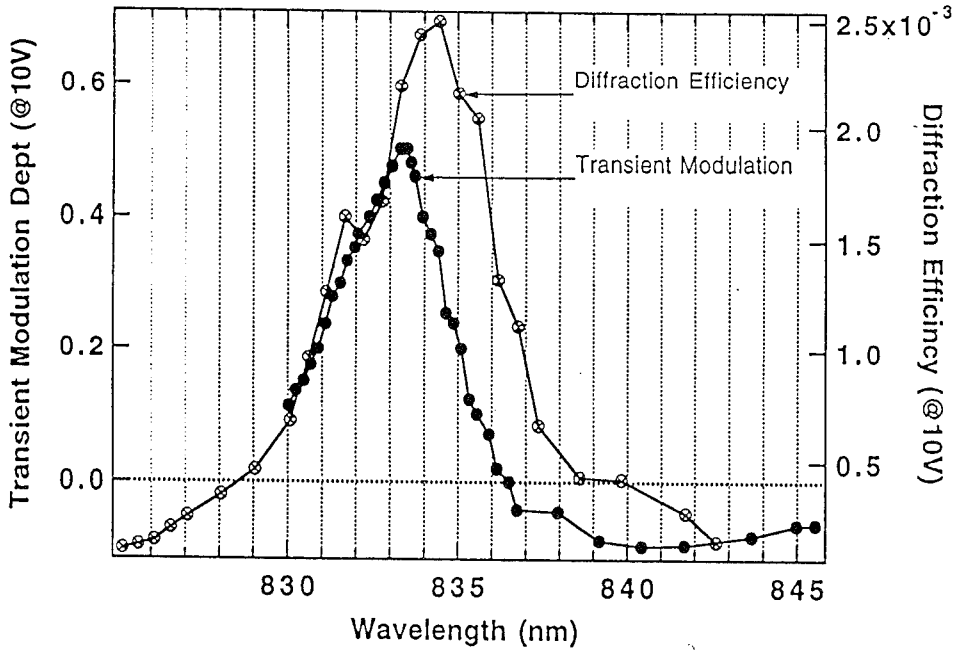


**Figure 7 Spectral Response of the Transient Electroabsorption and Four-Wave Mixing**

### *4.2.4. Four-Wave Mixing (FWM) Experiments .*

We then proceeded to perform FWM experiments to determine the spatial resolution and the diffraction efficiency of the device. In these experiments two coherent laser beams were used as writing beams. Because of the thin film nature of the device, the writing beams play the role of the readout beam too (see Figure 8) producing Raman-Nath diffracted beams. We studied the FWM properties of the device by measuring the first order diffracted beams:

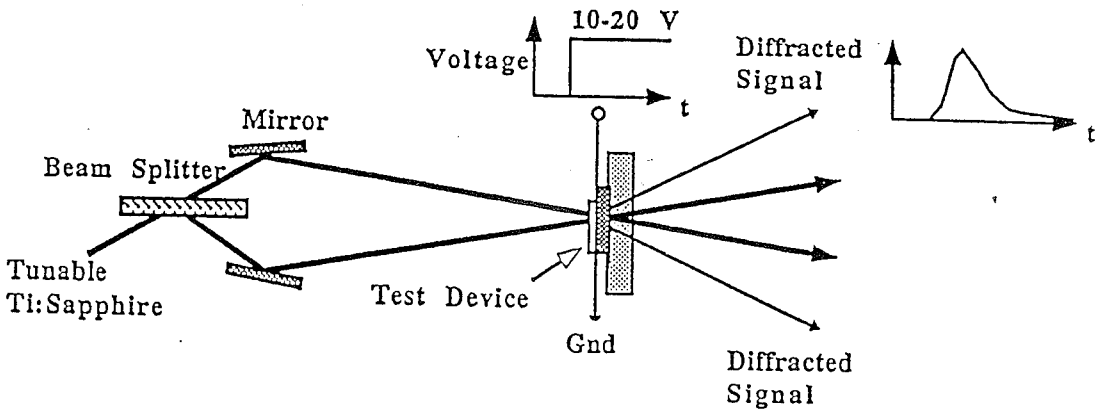


**Figure 8. Experimental Setup for measuring the Four-Wave Mixing Response**

*4.2.5 Diffraction efficiency*

Diffraction efficiency was monitored in real time using a high speed digital oscilloscope. Figure 9 shows the oscilloscope traces of the diffracted beam, the transmitted beam and the applied voltage step. As shown the transmitted beam undergoes a fast change (limited by the 4μs response time of the detection system) followed by a gradual decrease because of charge screening (explained above). *The diffracted beam however builds up slower because the Photorefractive grating has to be formed by spatially varying charge screening.* This observation confirms that the effect is due to photorefraction. *The diffraction efficiency was measured by measuring the ratio of the peak of the diffracted power to the transmitted beam .*

Diffraction efficiency was measured as a function of the wavelength as well as the length of the applied pulse. Figure 7 shows the spectral response of the diffraction efficiency at ± 10V applied voltage. The peak diffraction efficiency was increased from 0.2% at this voltage to 3.3% at ±70V (see Figure 10).

It was also clear that the diffraction efficiency depended on the pulse width, the duty cycle and the intensity. In Figure 10, the diffraction efficient as a function of the pulse width is shown indicating a 3.3% peak at approximately 0.8 ms width. The diffraction efficiency dropped at lower and higher pulse widths but could be recovered by for example changing the duty cycle. These experimental results have significant impact on systems design and will be followed up and addressed in details in Phase II. In particular we evaluate novel methods involving interface design that are expected to produce high diffraction efficiencies with shorter pulse widths. This will reduce possible stringent requirements on output plane detector arrays at low photon densities.

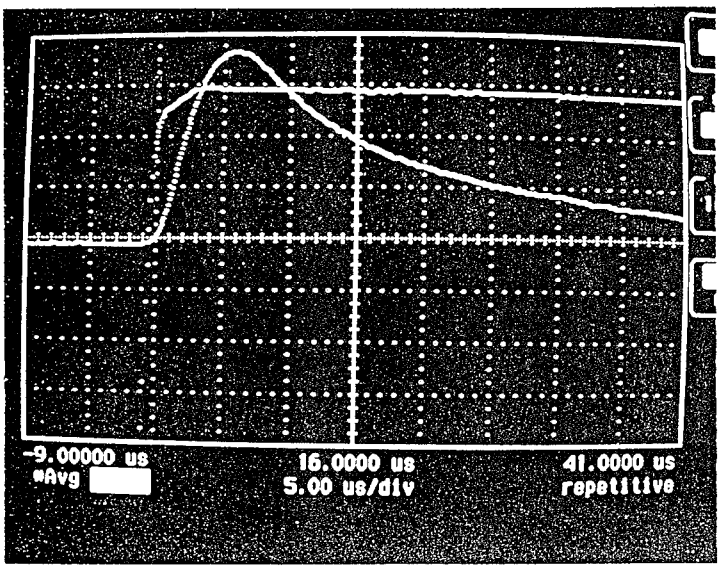


Figure 9. The Oscilloscope Trace of the Diffracted Beam

*4.2.6. Spatial Resolution*

By varying the angle between the two beams and measuring the value of the diffraction efficiency we determined the spatial resolution of the device. Figure 11 shows the results. For large grating spacing the diffraction efficiency is flat. As the grating spacing is reduced below 10μm the diffraction efficiency drops sharply. At the grating spacing Λ of approximately 5μm the diffraction efficiency drops to half its maximum value. This value defines the spatial resolution: ~5μm. In Figure 11 we fit the diffraction efficiency η according to the generic photorefractive response:

$$\eta=\eta_0/[1+(\Lambda/\Lambda_0)^2]^2$$

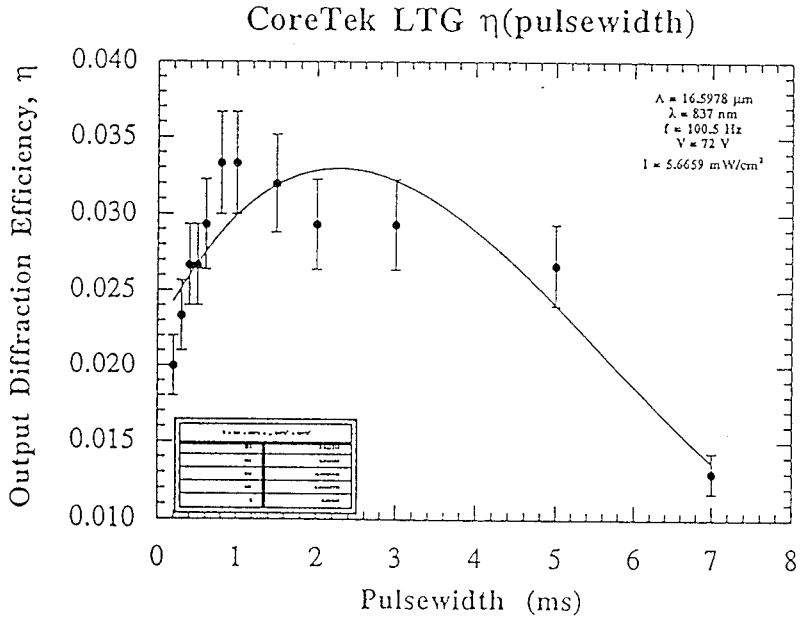


Figure 10. Diffraction efficiency as a function of the pulse-width.

The best fit to experimental data provides a value of $\Lambda_o$ = 2.8μm for the spatial resolution. This definition is consistent with the definition of half-maximum in electric field E distribution developed for PROM devices [4]. A half maximum field (E) translates into a drop by a factor of four in diffraction efficiency (since $\eta \sim E^2$).

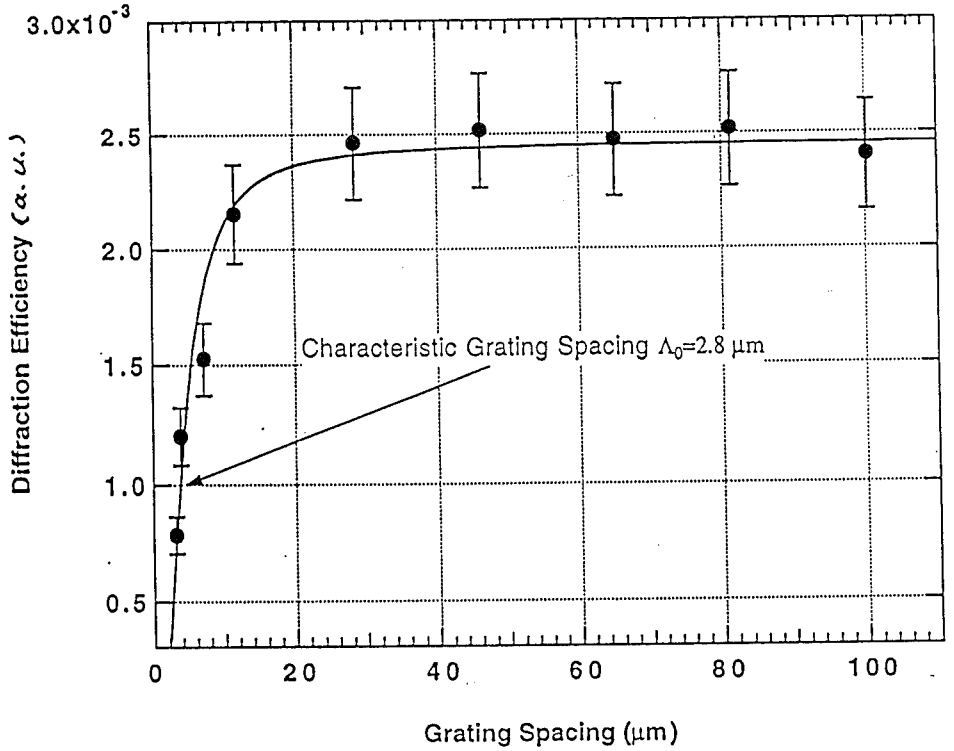


**Figure 11. Diffraction Efficiency Versus Grating Spacing in CoreTek's Shows a Spatial Resolution of 2.8μm to 6μm (see text).**

*4.2.7. Photorefractive Speed*

Speed of photorefraction scales nearly linearly with intensity (sometimes sublinearly) [8]. As an independent way to confirm the photorefractive nature of the effect and to characterize the intensity dependence of the effect, FWM response time was measured as a function of intensity. A characterization over an intensity range of nearly two orders of magnitude is shown in Figure 12. The best fit to the data shows that the response time follows a $I^{-0.83}$ rule. Extrapolating this data to 1W/cm$^2$ shows a 400ns response time at 1W/cm$^2$. *This is three time faster than the best reported number in MQW based devices (by AT&T).* In Phase II we will compare these results more deeply and consider effects such as the field distribution and field dependence of the response time that might have affected our improved response time.

We also observed that when the light intensity is increased beyond the 3μs response time, the response time saturates to about 2μs and the diffraction efficiency drops. We believe this is caused by the high contact resistivity of the device causing large RC time constant. This is evident in the transient electroabsorption experiments (Figure 6) where the rise time is solely affected by the RC time constant. As shown the response time of the electroabsorption is about 2μs indicating a limiting RC time constant. In Phase II better electrical contacts and thicker p- and n- type layers will be considered to improve the response time even further.

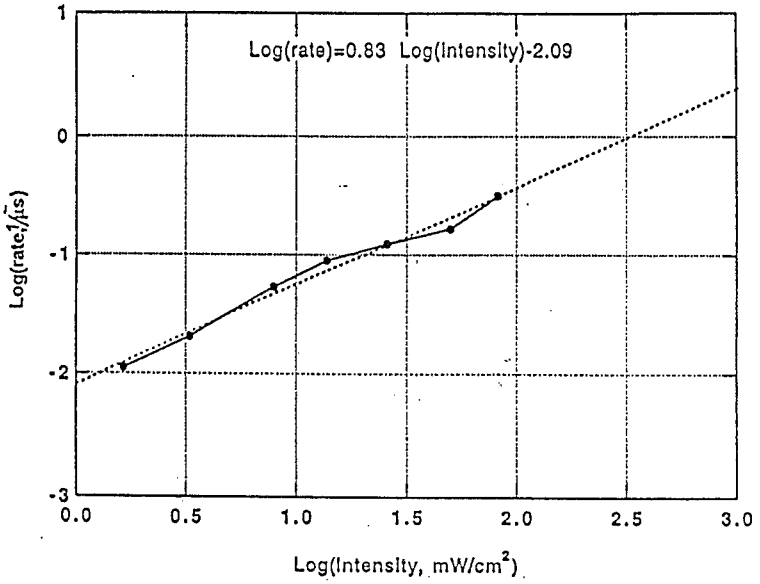


**Figure. 12 Response Time Versus Intensity in CoreTek's PR-SLM device.**

*4.8-Voltage Dependence of FWM*

Scaling of the diffraction efficiency with voltage were also studied. In Figure 13 our studies of up to 200V p-p is shown. Note that the diffraction efficiency drops for intensities above 72 V. We are currently developing simple models to explain the behavior of the device. Also note that the diffraction efficiency peak is 2.5% not 3.3%. This is because the diffraction efficiency drops gradually by going to higher intensities, as was the case in the two experiments.

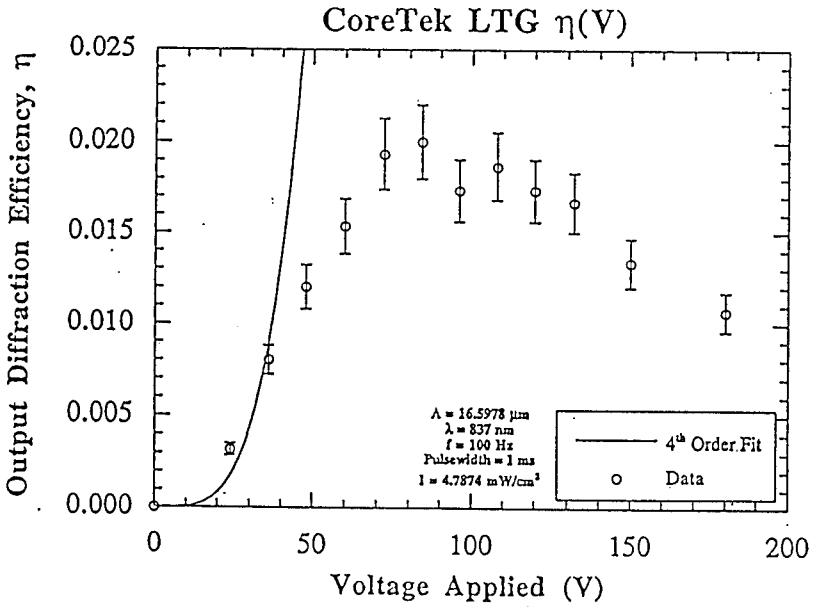


**Figure 13 Dependence of the diffraction efficiency on applied voltage.**

## 4.3-CoreTek's Photorefractive Device In Reflection Mode

After full characterization of the device in the transmission mode we deposited a thin Al mirror on the top of the device to be able to operate the device in reflection mode. In this mode the device is more difficult to test since the high reflectivity of the back mirror causes strong Fabry-Perot effects that affect the reflected beam intensities and therefore the diffraction efficiency. A preliminary characterization of the device was then performed by measuring the diffraction efficiency as a function of the wavelength and as a function of the incident angle of the two writing beams. We observed and studied the effect of Fabry-Perot oscillation on diffraction efficiency and describe them qualitatively.

In addition we also observed Extend optical storage in our devices up to 10ms and beyond. We will present these results also.

### 4.3.1 Diffraction Efficiency Verses Wavelength in Reflection Mode

We measured the diffraction efficiency of the device in reflection as a function of wavelength. In these experiment we kept the angle between two beams at 13 degrees and used 30V peak voltage. For every wavelength we also measured the reflectance of one of the writing beams. In Figure 14 we plot the reflectivy and the diffraction efficiency as a function of the wavelength. As shown both the reflectance and the diffraction efficiency exhibit oscillatory behavior that correlate well with each other and with the calculated Fabry-Perot phase that is calculated and shown in solid. Experimental results shows however that in reflection the Fabry-Perot mode structure is influenced greatly by the mode structure of the device. The full theoretical explanation of these oscillations including the out-of-phase behavior of the reflectivity and the diffraction efficiency are beyond the scope of this project.

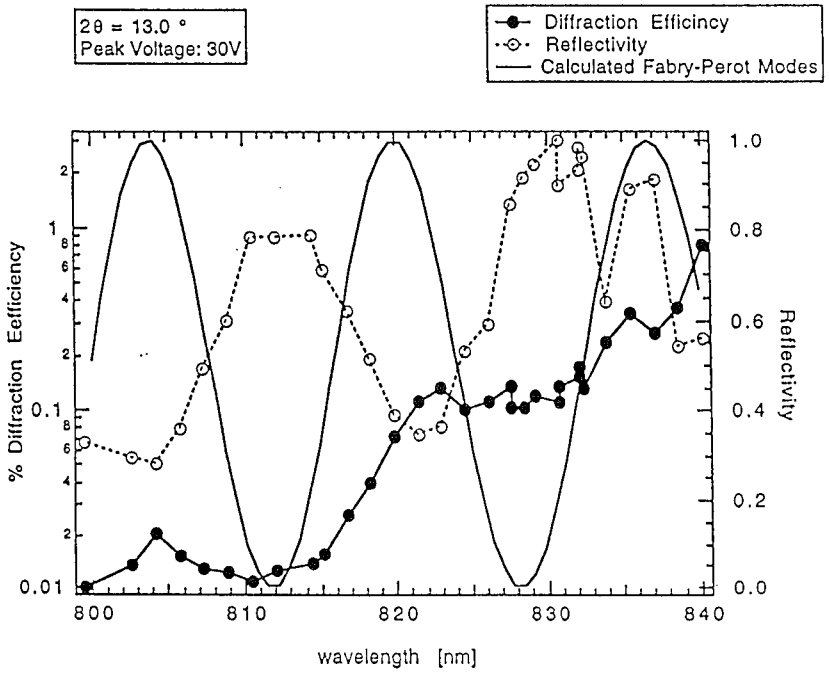


**Figure 14. Diffraction efficiency, Reflectance and Calculated Fabry-Perot Phase as a function of Wavelength.**

### 4.3.2 Diffraction Efficiency Verses Angle of Incident in the Reflection Mode

In the next step we performed four-wave mixing experiments as a function of the angle of incident while keeping the angle between the writing beams and the wavelength fixed (at 835.7nm). Figure 15 shows the experimentally measured values of diffraction efficiency and reflectivity. As shown there is a clear evidence of out-of-phase of oscillations in the data. As shown the diffraction efficiency varies by almost an order of magnitude as the angle of incidence tunned over five degrees. This indicates that in such devices either an antireflection coating has to be used or the angle of incidence has to be optimized in a practical application.

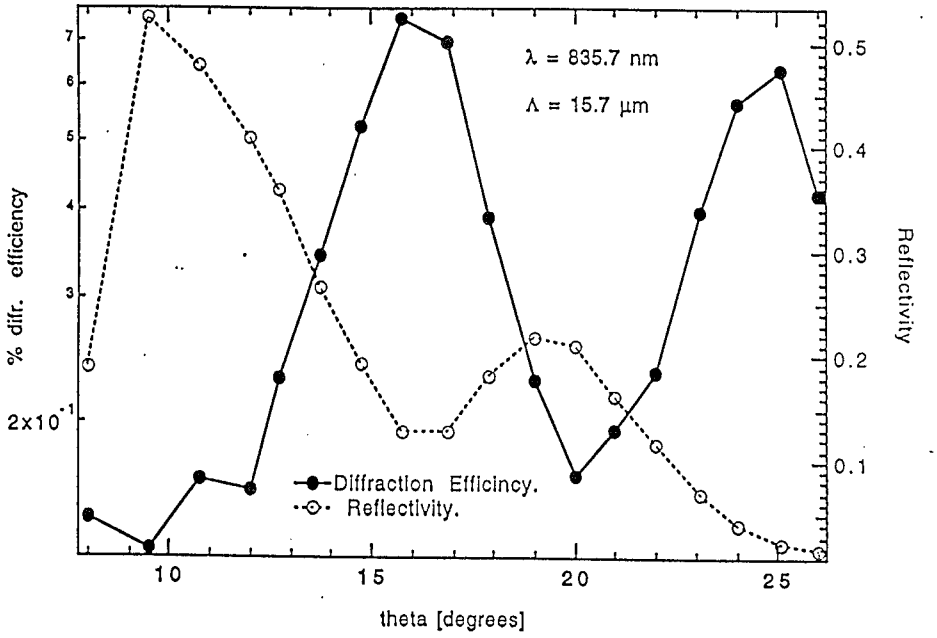


**Figure 15. Diffraction efficiency, Reflectance as a function of Angle of Incidence.**

### 4.3.3. Electrically Controllable Optical Storage in the Reflection Mode Device

In the preliminary experiments of these devices we observed a very long (>10ms) electrically switchable storage capability. This is demonstrated in Figure 16 where the diffraction efficiency remains "on" for a long time before decaying (lower curve) when the electric field is left "on" (upper curve). The efficiency can be switched off at any time by switching the electric field "off". This effect occurs only when higher voltages are applied and the intensity is within certain limits. Such an effect was also observed in MQW based devices[4], in this case the effect lasted only up to 25μs. In our device this effect is more than two orders of magnitude longer and as in the case of MQW device [4] remains unexplained.

This effect could be of significant importance and will be studied carefully in Phase II. In addition to possible applications to optical storage and image buffering, this property is important for its direct applications in optical correlation. It is generally advantageous to be able to keep the output signal at a steady level when it is being read out by the detector array in the output plane. The observation described here might provide a path in this direction and deserves a thorough study.

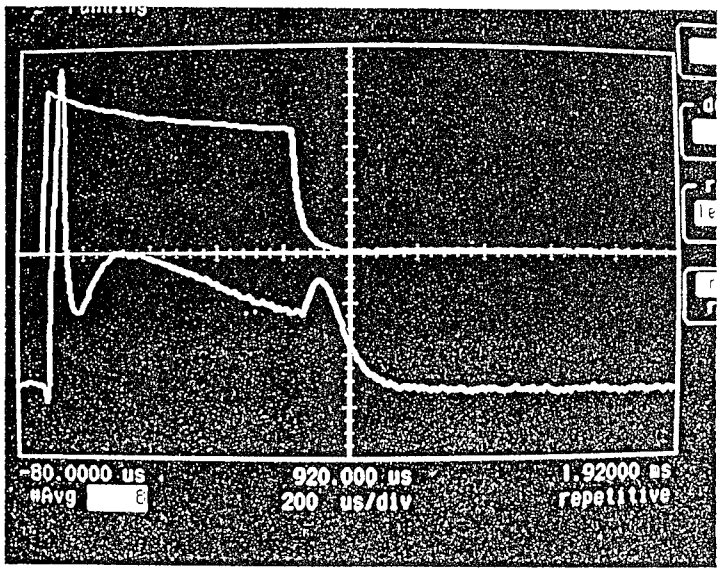


**Figure 16. Electrically Controllable Memory in LTG-GaAlAs Photorefractive Device.**

## 5. Conclusion

This Phase I has resulted in a novel high spatial resolution nonlinear optical technology taking advantage of LTG-GaAlAs materials alone. We showed it is possible to use the short diffusion length of photocarriers and the semiinsulating properties of these materials to develop devices that have the following unique and novel properties:

- *High Spatial Resolution*: A record spatial resolution of 5μm compared to 40μm respectively for today's state-of-the-art by AT&T and others (see Table 1). This means over 50 times higher processing throughput per unit area.

- *Fast Response Time*: A record fast response time of 3μs compared to 30μs for today's state-of-the-art by AT&T (@ 0.1W/cm$^2$). This means a factor of twenty improvement in device speed.

- *Longest Storage Time*: Storage time of over 10ms, compared to 20μs storage time in AT&T's devices.

- *Monolithic Structure:* Going well beyond the goals of Phase I, we exploited the extraordinary semiinsulating properties of LTG-GaAlAs to fabricate the first all LTG-GaAlAs PR-SLM device in a *semi-monolithic* form. This is a significant technology breakthrough allowing fabrication of *fully monolithic* devices in Phase II.

These devices can now be used in high throughput optical correlators with high speed pattern recognition applications. Other possible applications includes:

- Short pulse measurements,
- Realtime holography for mechanical vibration analysis
- Novelty filters for motion spectroscopy

etc.

In Phase II we propose to expand this effort by fabricating 100% LTG-GaAlAs monolithic devices and use them to build a novel Raman-Nath optical correlator for use in a wide range of commercial applications. CoreTek, Inc. has formed a team of end users and potential

investors that will benefit and support this project during Phase II and Phase III commercialization. Phase II funding in this project will greatly enhance CoreTek's efforts in pushing for commercialization of optical correlators.

## 6. References


1. Glass. A. M. Optics Letters Vol. 15 no 5 p.264
2. Partovi, A. et al., Appl. Phys. Lett. 62(5), 1 Feb. 1993, P. 464. and ref.s within.
3. Partovi, A. et al., Optics Lett. 18(11), 1 June. 1993, P. 906. and ref.s within.
4. Nolte, D. D. et al., Appl. Phys. Lett. 61(26), P. 3098
5. Nolte D. D. et al., Appl. Phys. Lett. 62(12), P. 1356
6. Goossen. K. W. et al. Technical Digest of LEOS '93 San Jose, CA. Paper SP1.4, p.662.
7. Tayebati, P. , Appl. Phys. Lett. 63(21), 22 Nov. 1993, p. 2878.
8. Tayebati, P. and L. Jauniskis Appl. Phys. Letts, Feb. 14 1994.